Journal of Solar Energy

Modular Reactor Model for the Solar Thermochemical Production of Syngas Incorporating Counter-Flow Solid Heat Exchange

Christoph P. Falter[1*], Andreas Sizmann[1], Robert Pitz-Paal[2]

[1]Bauhaus Luftfahrt, Willy-Messerschmitt-Straße 1, 85521 Ottobrunn, Germany

[*]corresponding author: christoph.falter@bauhaus-luftfahrt.net

andreas.sizmann@bauhaus-luftfahrt.net

[2]DLR, Institute of Solar Research

Linder Höhe, 51147 Köln, Germany

robert.pitz-paal@dlr.de

ABSTRACT

Recent progress in thermochemical reactor concepts, among them batch, particle and counter-rotating configurations, shows different approaches to heat recuperation and gas separation. An idealized physical analysis in search of best-efficiency potentials is required, that covers multiple degrees of freedom in configuration space from batch to quasi-continuous concepts.

A modular and generic solar thermochemical reactor model is thus presented that describes two-step redox reactions of solid pieces of reactant moving in counter flow between reduction and oxidation chambers to produce CO and H_2 from CO_2 and H_2O. The reactive material absorbs concentrated solar radiation in the reduction chamber and is then passed on to oxidation through a series of intermediate chambers, in which radiation energy is exchanged with colder oxidized elements travelling in the opposite direction. In this way, solid heat recovery is implemented which is essential to achieve high efficiencies. The reduction and oxidation reactions are modeled at constant temperatures and pressures in the reaction chambers and the heat exchanger efficiency is derived based on energy conservation involving radiation energy transfer between the elements and energy losses to the environment. The model can be adapted to a wide range of reactor concepts and is validated through a comparison of results with models presented in the recent literature.

The model is demonstrated in an upper-bound performance analysis with an example of a ceria system. With a length of the heat exchanger and a residence time of the elements therein chosen near their optimum combination, a heat exchanger efficiency of about 80% is reached. The energy balance of the system shows that the enthalpy of heating ceria and its reduction require the largest energy input. Using the minimum thermodynamic energy for the vacuum pump and gas separation, the physical potential of cycle efficiency at the modeled temperatures at a reduction oxygen partial pressure of 10^{-3} atm is 22% and may be increased to 33% at a partial pressure of 10^{-5} atm. With assumptions on practical energy requirements the efficiency is reduced to 16% at 10^{-3} atm. In order to quantify the dependence of the heat exchanger

efficiency on internal heat transfer characteristics, heat propagation by radiation and conduction through the reactive material and insulation is modeled in the exemplary case of a porous medium.

This model provides the basis for future analyses of reactor concepts including parameter studies of the number of heat exchanger chambers, the residence time and reaction temperatures.

Keywords:

- Solar fuel
- Redox cycle
- Heat recovery
- Model

NOMENCLATURE

$A_{\mathrm{he,ext}}$	External area of heat exchanger chamber facing the environment [m²]
$A_{\mathrm{he,ext,total}}$	Total external area of heat exchanger facing environment [m²]
$A_{\mathrm{he,int}}$	Internal area of heat exchanger chamber half facing other half of chamber [m²]
$A_{\mathrm{he,int,total}}$	Total internal area of heat exchanger [m²]
c_{CO}	Concentration of CO [-]
$c_{p,\mathrm{CeO_2}}$	Heat capacity of ceria at constant pressure [J mol^{-1} K^{-1}]
$c_{p,\mathrm{CO_2}}$	Heat capacity of CO_2 at constant pressure [J mol^{-1} K^{-1}]
$c_{p,\mathrm{O_2}}$	Heat capacity of O_2 at constant pressure [J mol^{-1} K^{-1}]
$f_{\mathrm{CO_2}}$	Molar flow rate of CO_2 into oxidation chamber as a multiple of δ_{red} [-]
ΔG_{O_2}	Oxygen molar free energy [J mol^{-1}]

ΔH_O	Partial molar enthalpy of oxygen [J mol^{-1}]
$\Delta H_{\mathrm{CeO_2}}$	Reduction enthalpy of ceria [J mol^{-1}]
ΔH_{red}	Reduction enthalpy [J mol^{-1}]
K	Thermodynamic equilibrium constant [-]
K_{CO_2}	Thermodynamic equilibrium constant for CO_2 splitting reaction [-]
L_{chamber}	Length of heat exchanger chamber [m]
m	Mass of ceria element [kg]
$\dot{n}_{\mathrm{CeO_2}}$	Molar flow rate of ceria [mol s^{-1}]
$\dot{n}_{\mathrm{CO}}$	Molar flow rate of CO [mol s^{-1}]
$\dot{n}_{\mathrm{CO_2}}$	Molar flow rate of CO_2 [mol s^{-1}]
$\dot{n}_{\mathrm{CO_{2,i}}}$	Molar flow rate of carbon dioxide entering the oxidation chamber [mol s^{-1}]
$\dot{n}_{\mathrm{O_2}}$	Molar flow rate of oxygen [mol s^{-1}]
$\dot{n}_{\mathrm{total}}$	Total gas flow rate in oxidation chamber [mol s^{-1}]
p_0	Ambient pressure relative to standard state [-]
$\bar{p}_{CO}$	Carbon monoxide partial pressure relative to standard state [-]
$\bar{p}_{CO_2}$	Carbon dioxide partial pressure relative to standard state [-]
$\bar{p}_{O_2}$	Oxygen partial pressure relative to standard state [-]
P_{aux}	Auxiliary power needed to operate reactor [W]
$P_{\mathrm{pump,vacuum}}$	Power required for operation of vacuum pump [W]

$P_{\mathrm{sep,CO/CO_2}}$	Power required for gas separation of CO/CO_2-mixture [W]
$\dot{Q}_{\mathrm{heat,CeO_2}}$	Solar power needed to heat ceria [W]
$\dot{Q}_{\mathrm{heat,CO_2}}$	Solar power needed to heat CO_2 [W]
$\dot{Q}_{\mathrm{heat\ exchange}}$	Net rate of energy transferred between ceria element in upper chamber half and lower chamber half [W]
$\dot{Q}_{\mathrm{loss,conv}}$	Power lost by convection from heat exchanger chamber half [W]
$\dot{Q}_{\mathrm{loss,rad}}$	Power lost by radiation from heat exchanger chamber half [W]
$\dot{Q}_{\mathrm{products}}$	Power recovered from gaseous products [W]
$\dot{Q}_{\mathrm{red,CeO_2}}$	Solar power needed to reduce ceria [W]
$\dot{Q}_{\mathrm{rerad}}$	Rate of radiation heat losses from the reduction chamber [W]
$\dot{Q}_{\mathrm{solar}}$	Solar power input to reactor [W]
$\mathcal{R}$	Ideal gas constant [J mol^{-1} K^{-1}]
ΔS_O	Partial molar entropy of oxygen [J mol^{-1} K^{-1}]
t	Time [s]
Δt	Residence time in heat exchanger chamber [s]
T	Temperature [K]
T_0	Ambient temperature [K]
T_H	Reduction temperature [K]
$T_{k,\mathrm{l}}$	Temperature of lower half of *k*-th heat exchanger chamber [K]
$T_{k,\mathrm{u}}$	Temperature of upper half of *k*-th heat exchanger chamber [K]

T_L	Oxidation temperature [K]
T_{pump}	Temperature of vacuum pump [K]
T_{wall}	Temperature of heat exchanger wall facing surroundings [K]

50

51

52 **GREEK LETTERS**

α	Convective heat transfer coefficient at heat exchanger wall
δ	Oxygen nonstoichiometry of ceria
δ_{ox}	Oxygen nonstoichiometry of oxidized ceria
δ_{red}	Oxygen nonstoichiometry of reduced ceria
$\varepsilon_{\text{wall}}$	Emissivity of heat exchanger wall facing the environment
ε_{u}	Emissivity of ceria element in upper chamber half
ε_{l}	Emissivity of ceria element in lower chamber half
η	Efficiency (concentrated solar to chemical energy stored in CO)
η_{abs}	Absorption efficiency of reactor
η_{gasrec}	Recuperation efficiency of gases leaving the reduction and oxidation chambers
η_{he}	Heat exchanger efficiency
σ	Stefan-Boltzmann constant [W m^{-2} K^{-4}]

53

54

1. INTRODUCTION

The transportation sector today relies almost exclusively on liquid fuels derived from refinement of fossil crude oil (International Energy Agengy, 2014). Besides historic reasons, this is due to their superior energy density, handling and storage properties compared to other fuels. Among the different means of transport, especially aviation and heavy-duty road and sea traffic rely heavily on these fossil fuels because of their inherent high restrictions with respect to the energy and power density of the fuel. For these applications, a change towards electrification is not as easy to implement as for light-duty road transport where first electro-mobility solutions have started to appear on the market already. Additionally, rising concerns about climate change, partly due to emissions from the transportation sector, drive the search for alternatives for vehicle propulsion. As the demand for personal travel is very likely to increase (U.S. Energy Information Administration, 2014), the production of a sustainable energy-dense fuel is the key enabler for greenhouse gas reductions in the transportation sector of the future. Especially the conversion of solar energy, the most abundant renewable energy source on earth, to liquid fuels appears to be an attractive path (Kim et al., 2012; Roeb et al., 2011; Romero and Steinfeld, 2012; Stechel and Miller, 2013).

Compared to other approaches of producing solar fuels, based on photochemistry or electrochemistry, processes based on thermochemistry promise thermodynamic advantages (Steinfeld and Epstein, 2001). Using concentrated solar energy, chemical reactions are driven to split carbon dioxide and water into syngas, a mixture of hydrogen

and carbon monoxide, which is further processed in a Fischer-Tropsch process into liquid hydrocarbon fuels. For the implementation of thermochemical cycles, different solar reactor concepts exist that use redox cycles of metal oxides, *e.g.* ceria, to produce syngas or its constituents. Depending on the chemistry of the process, *i.e.* whether the reactions are taking place in a stoichiometric or non-stoichiometric way, different requirements have to be met. In the former case, a phase change of the metal oxide takes place that necessitates high-temperature separation of the products to avoid their recombination (Loutzenhiser et al., 2010). Although many stoichiometric processes show a high theoretical efficiency potential, some of them have shown to suffer from technical drawbacks that have prevented further development so far.

In the past couple of years, the development of solar reactors has included non-stoichiometric redox reactions of ceria that do not fully reduce the metal oxide but rather stop at an earlier stage to retain the reactive material in a solid phase(Bader et al., 2013; Chueh and Haile, 2009; Chueh et al., 2010; Furler et al., 2012a; Hao et al., 2013). This does not allow achieving the same level of reduction and therefore yield per mass of oxide per cycle. However, contrary to the Zn/ZnO-cycle, for example, products are not prone to recombine which allows a simpler reactor and process design, as now only a single vessel is minimally required. First experiments show promising results with respect to technical viability and achieved cycle efficiency (Chueh et al., 2010; Furler et al., 2014, 2012a).

Among the reactor concepts working with non-stoichiometric redox reactions of metal oxides, three different approaches may be distinguished. Firstly, a continuously

rotating and heat recuperating concept was presented by Diver et al. (Diver et al., 2008) where rings of reactive material are heated and reduced on one side and oxidized on the other. Through the counter-rotation of adjacent rings, heat recuperation is achieved. Secondly, in 2009, a batch reactor concept was developed at ETH Zurich that uses ceria for syngas production (Chueh et al., 2010). Inert gases are used for the reduction of the oxygen partial pressure which also limits the efficiency potential, as shown by Ermanoski et al. in (Ermanoski et al., 2013). Thirdly, a particle reactor concept has been presented that uses a continuous feeding process, counter-flow heat exchange and gas separation through packed beds of particles (Ermanoski et al., 2013). Besides these three concepts, recently, an isothermal reactor concept has been proposed that tries to alleviate the necessity for solid heat recuperation through a pressure swing process operating at constant temperature throughout reduction and oxidation (Bader et al., 2013; Hao et al., 2013). However, the operation at a constant high temperature makes very high gas recuperation efficiencies necessary to achieve high overall cycle efficiency. In fact, Bader et al. (Bader et al., 2013) conclude that the introduction of an additional temperature swing will increase the cycle efficiency over the isothermal concept. The development of solid heat recuperation concepts as modeled in this paper is therefore seen to be crucial for highly efficient reactors.

From the different concepts and their analyses shown above, prerequisites for a highly efficient reactor concept can be deduced, *i.e.* heat recuperation and gas separation, besides others, as also shown and analyzed in previous studies on reactor concepts (Bader

et al., 2013; Ermanoski et al., 2013; Felinks et al., 2014; Lapp and Lipinski, 2014; Lapp et al., 2013, 2012).

As analyses so far have either focused on a specific reactor concept or on basic considerations without conceptual implementation, it is worth investigating a reactor model that is able to explore upper-bound performance limits and specific concepts in a wide design space, in order to gain further insight into crucial aspects for achieving high efficiencies. With respect to a related analysis that focuses on a particle reactor concept (Ermanoski et al., 2013) which is used for the validation of the presented model, further generalization and development is sought through the use of a realistic pump efficiency and modeling of the oxidation reaction and the heat exchange. The presented model in this analysis is therefore a generic approach to parametrically describe the most important aspects of solar reactors and enables to investigate very different concepts from the batch-operated processes to quasi-continuous counter-flow arrangements. In the following, the model is presented and demonstrated with an exemplary system. This will be the basis to gain more insight into favorable reactor design in the future through a variation of the parameters, *e.g.* the number of heat exchanger chambers or residence time.

2. PHYSICAL REACTOR CONCEPT AND NUMERICAL MODEL DESCRIPTION

A physical generic reactor concept for a two-step thermochemical process is described consisting of a reduction chamber, intermediate chambers for heat exchange and an oxidation chamber (Fig. 1). With initial species concentrations and constant temperatures in the reaction chambers, equilibrium thermodynamics and species conservation are used to calculate the nonstoichiometry and the amount of fuel produced. The evolving temperatures in the heat exchanger are calculated with a lumped parameter model that applies conservation of energy between the thermal energy stored in the ceria elements, internal radiative heat exchange and energy lost to the surroundings by radiation and convection.

The reactor concept consists of (n-2) heat exchanger chambers in order to allow the description of technically feasible heat exchanger concepts working with experimentally proven sizes of elements of reactive material. For example, the batch-reactor concept (Chueh et al., 2010; Furler et al., 2014, 2012a) could be improved through the introduction of a small number of heat exchanger chambers operating between a reduction and oxidation chamber. In the analysis of the example system below, ceria elements of 1 kg are used as is roughly the case in (Furler et al., 2014).

Without loss of generality of the approach, we consider nonstoichiometric ceria as the reactive material. Application to other materials is straightforward if the respective

material properties are known. Solid pieces of ceria are reduced at an elevated temperature T_H and a reduced oxygen partial pressure p_{O_2}. The level of oxygen nonstoichiometry is increased from δ_{ox} after oxidation to δ_{red} after reduction, see Eq. 1.

$$\frac{1}{\delta_{red}-\delta_{ox}}\mathrm{CeO}_{2-\delta_{ox}} \rightarrow \frac{1}{\delta_{red}-\delta_{ox}}\mathrm{CeO}_{2-\delta_{red}} + \frac{1}{2}\mathrm{O}_2 \quad (1)$$

$$\frac{1}{\delta_{red}-\delta_{ox}}\mathrm{CeO}_{2-\delta_{red}} + \mathrm{H_2O} \rightarrow \frac{1}{\delta_{red}-\delta_{ox}}\mathrm{CeO}_{2-\delta_{ox}} + \mathrm{H_2} \quad (2)$$

$$\frac{1}{\delta_{red}-\delta_{ox}}\mathrm{CeO}_{2-\delta_{red}} + \mathrm{CO_2} \rightarrow \frac{1}{\delta_{red}-\delta_{ox}}\mathrm{CeO}_{2-\delta_{ox}} + \mathrm{CO}$$

$$\mathrm{H_2O} \rightarrow \tfrac{1}{2}\mathrm{O_2} + \mathrm{H_2} \quad (3)$$

$$\mathrm{CO_2} \rightarrow \tfrac{1}{2}\mathrm{O_2} + \mathrm{CO}$$

When the reduction reaction is completed, the ceria pieces are passed on to the oxidation chamber through the heat exchanger, where heat is exchanged through radiation with oxidized pieces travelling in the lower half of chambers in the opposite direction. In each heat exchanger chamber, the pieces have a residence time Δt before they pass on to the next one. Convection within each chamber half is assumed to be small and is therefore neglected. Heat between the ceria pieces is solely exchanged through radiation. The upper half of the chambers is assumed to be separated from the lower one through a barrier in order to ensure separation of gases, preventing recombination and thus enabling high efficiencies in the reactor. The separating wall is assumed not to hinder heat exchange between the reduced and oxidized ceria pieces, which should be

fulfilled for the separating wall having high thermal conductivity and emissivity, and being in direct contact with either piece in steady state operation.

In the oxidation chamber, the reduced ceria is contacted with carbon dioxide to reoxidize the material (see Eqs. 2). Carbon dioxide is split into oxygen and carbon monoxide, where the oxygen enters the ceria lattice and carbon monoxide is captured. Oxidation can also be achieved with water steam to produce hydrogen or with a mixture of both oxidants to produce syngas directly (Furler et al., 2012b). In the following, CO_2 shall be used as an oxidant without loss of generality. In theory, the stoichiometric amount of oxidant could be supplied to the reactor to produce pure carbon monoxide. For reasons of thermodynamic driving force and kinetics, however, an excess amount of oxidant is supplied, resulting in a mixture of CO and CO_2 at the exit of the oxidation chamber. As the Fischer-Tropsch (FT) reactor works best with only small amounts of CO_2 contamination in the syngas and in order to recycle excess oxidant, separation of the CO/CO_2 gas is performed.

For the reduction of oxygen partial pressure, a pump is assumed to evacuate the reduction chamber to a defined value of p_{O_2}. Additionally, the second-to-last chamber (labeled "*n*-1" in Fig. 1) is assumed to be evacuated in order to prevent oxidation of the ceria pieces before the oxidation chamber. Were this additional evacuation not implemented, a pressure profile with a linear progression would be obtained, leading to partial oxidation of the reduced ceria pieces in the intermediate heat exchanger

chambers. The consequently required distributed collection of gases would complicate the reactor concept and is therefore rather undesirable.

The oxygen nonstoichiometry of the reduction reaction has been experimentally analyzed by Panlener *et al.* (Garnier et al., 1975) as a function of oxygen partial pressure and temperature. A function fitted to the experimental data is used to calculate δ_i in the reduction chamber (Ermanoski et al., 2013). The oxidation reaction is the sum of the reverse reduction reaction (Eq. 1) and carbon dioxide splitting (Eq. 3). The former can be described by

$$\Delta G_{\mathrm{O}_2}(T_\mathrm{L}, \delta_\mathrm{ox}) \quad = \quad \mathcal{R} T_\mathrm{L} \ln K = \mathcal{R} T_\mathrm{L} \ln \bar{p}_{\mathrm{O}_2}, \tag{4}$$

where $\Delta G_{\mathrm{O}_2}(T_\mathrm{L}, \delta_\mathrm{f})$ is the oxygen molar free energy, T_L the oxidation temperature, K the thermodynamic equilibrium constant of the overall reaction and $\bar{p}_{O_2}$ the oxygen partial pressure relative to the standard state of 1 atm. The oxygen partial pressure can be derived from

$$K_{\mathrm{CO}_2} \quad = \quad \frac{\bar{p}_\mathrm{CO} \bar{p}_{\mathrm{O}_2}^{\frac{1}{2}}}{\bar{p}_{\mathrm{CO}_2}}. \tag{5}$$

The equilibrium partial pressure of CO_2 is calculated from a mass balance of the closed system

$$\bar{p}_{\mathrm{CO_2}} = \frac{\dot{n}_{\mathrm{CO_{2,i}}} - (\delta_{\mathrm{red}} - \delta_{\mathrm{ox}})\dot{n}_{\mathrm{CeO_2}}}{\dot{n}_{\mathrm{total}}} = \frac{\left(f_{\mathrm{CO_2}}\delta_{\mathrm{red}} - (\delta_{\mathrm{red}} - \delta_{\mathrm{ox}})\right)\dot{n}_{\mathrm{CeO_2}}}{\dot{n}_{\mathrm{total}}}. \quad (6)$$

212

213 $\dot{n}_{\mathrm{CO_{2,i}}}$ is the molar flow rate of CO_2 entering the oxidation chamber, $(\delta_{\mathrm{red}} - \delta_{\mathrm{ox}})\dot{n}_{\mathrm{CeO_2}}$ is
214 the molar flow rate of CO produced (and CO_2 consumed) and $\dot{n}_{\mathrm{total}}$ the total molar flow
215 rate of gases. The partial pressure of CO is

$$\bar{p}_{\mathrm{CO}} = \frac{(\delta_{\mathrm{red}} - \delta_{\mathrm{ox}})\dot{n}_{\mathrm{CeO_2}}}{\dot{n}_{\mathrm{total}}}. \quad (7)$$

216

217 Solving Eq. (5) for the partial oxygen pressure gives

$$\bar{p}_{O_2} = \left(\frac{K_{\mathrm{CO_2}}\bar{p}_{\mathrm{CO_2}}}{\bar{p}_{\mathrm{CO}}}\right)^2. \quad (8)$$

218

219 Putting Eq. (8) into Eq. (4), inserting Eqs. (6-7) and rewriting the partial molar free
220 energy of lattice oxygen as a sum of enthalpy and entropy gives

$$\Delta H_{\mathrm{O}}(T_{\mathrm{L}}, \delta_{\mathrm{ox}}) - T_{\mathrm{L}}\Delta S_{\mathrm{O}}(T_{\mathrm{L}}, \delta_{\mathrm{ox}}) = \mathcal{R}T_{\mathrm{L}} \ln\left(\frac{K_{\mathrm{CO_2}}\bar{p}_{\mathrm{CO_2}}}{p_{\mathrm{CO}}}\right) \quad (9)$$

$$= \mathcal{R}T_{\mathrm{L}} \ln\left(\frac{K_{\mathrm{CO_2}}\left(f_{\mathrm{CO_2}}\delta_{\mathrm{red}} - (\delta_{\mathrm{red}} - \delta_{\mathrm{ox}})\right)}{(\delta_{\mathrm{red}} - \delta_{\mathrm{ox}})}\right), \quad (10)$$

221

222 where ΔH_{O}, ΔS_{O} and $K_{\mathrm{CO_2}}$ are known functions of temperature and nonstoichiometry.

By specifying the rate of CO_2-supply f_{CO_2} and δ_{red} (through a fitted function to experimental values), the above equation can then be solved for δ_{ox}.

Energy balance

Energy that is required to move ceria is neglected, as in (Ermanoski et al., 2013) it has been shown to be a negligible amount for the case of ceria particles. Energy available from the exothermic oxidation reaction is assumed to stabilize the ceria temperature in the oxidation chamber where there is no solar energy input and otherwise to be lost.

The overall energy balance of the system is

$$\dot{Q}_{solar} + P_{aux} - \dot{Q}_{heat,CeO_2} - \dot{Q}_{red,CeO_2} - \dot{Q}_{heat,CO_2} + \dot{Q}_{products} - \dot{Q}_{rerad} - P_{pump,vacuum} - P_{sep,CO/CO_2} = 0 \quad (11)$$

The solar power input to the reactor is

$$\dot{Q}_{solar} = \frac{1}{\eta_{abs}}\left(\dot{Q}_{heat,CeO_2} + \dot{Q}_{red,CeO_2} + \dot{Q}_{heat,CO_2} - \dot{Q}_{products}\right), \quad (12)$$

where η_{abs} is the absorption efficiency of the solar reduction chamber and is calculated with the assumption of a well-insulated blackbody cavity, leading to reradiation losses of $\dot{Q}_{rerad} = (1 - \eta_{abs})\dot{Q}_{solar}$.

$\dot{Q}_{heat,CeO_2}$ is the rate of heat required to increase the temperature of the oxidized ceria piece from the temperature at the exit of the heat exchanger to the reduction temperature,

$$\dot{Q}_{\mathrm{heat,CeO_2}} = (1-\eta_{\mathrm{he}})\dot{n}_{\mathrm{CeO_2}} \int_{T_\mathrm{L}}^{T_\mathrm{H}} c_{p,\mathrm{CeO_2}}(T)\,\mathrm{d}T. \quad (13)$$

The required power input to heat ceria is reduced by the amount of heat recovered from the solid phase in the heat exchanger with an efficiency of η_{he} which is defined as

$$\eta_{\mathrm{he}} = \frac{\int_{T_\mathrm{L}}^{T_{2,\mathrm{l}}} c_{\mathrm{p,CeO_2}}(T)\mathrm{d}T}{\int_{T_\mathrm{L}}^{T_\mathrm{H}} c_{\mathrm{p,CeO_2}}(T)\mathrm{d}T}, \quad (14)$$

where $T_{2,\mathrm{l}}$ is the temperature of the ceria piece at the end of the heat exchanger before entering the reduction chamber.

$\dot{Q}_{\mathrm{red,CeO_2}}$ is the rate of energy required to reduce the material from δ_{ox} to δ_{red}

$$\dot{Q}_{\mathrm{red,CeO_2}} = \dot{n}_{\mathrm{CeO_2}}\Delta H_{\mathrm{red}} = \dot{n}_{\mathrm{CeO_2}} \int_{\delta_{\mathrm{ox}}}^{\delta_{\mathrm{red}}} \Delta H_{\mathrm{CeO_2}}(\delta)\,\mathrm{d}\delta. \quad (15)$$

$\Delta H_{\mathrm{CeO_2}}$ is only weakly dependent on temperature and pressure and is thus taken to be a function of the nonstoichiometry only. Values for the reduction enthalpy as a function of oxygen nonstoichiometry are taken from Panlener *et al.* (Garnier et al., 1975).

$\dot{Q}_{\mathrm{heat,CO_2}}$ is the power to heat CO_2 from ambient conditions to the oxidation temperature

$$\dot{Q}_{\mathrm{heat,CO_2}} = \dot{n}_{\mathrm{CO_2}} \int_{T_0}^{T_L} c_{p,\mathrm{CO_2}}(T)\mathrm{d}T. \quad (16)$$

The properties of CO_2 and all other gases have been calculated with tables from Engineering Toolbox, 2014.

$\dot{Q}_{\text{products}}$ is the power that can be recovered from the gases leaving the reduction and oxidation zones (O_2, CO, CO_2) with an efficiency of η_{gasrec}.

$$\dot{Q}_{\text{Products}} = \eta_{\text{gasrec}} \left(\dot{n}_{\text{CO}} \int_{T_0}^{T_L} c_{p,\text{CO}}\,(T)\mathrm{d}T + \dot{n}_{\text{CO}_2} \int_{T_0}^{T_L} c_{p,\text{CO}_2}\,(T)\mathrm{d}T + \dot{n}_{\text{O}_2} \int_{T_0}^{T_L} c_{p,\text{O}_2}\,(T)\mathrm{d}T \right). \quad (17)$$

A distinction is made in the calculation of the pumping power between the idealized case of isothermal pumping and a more practically relevant case based on data from a pump manufacturer. In both cases, the released oxygen in the reduction chamber and the oxidant lost through the opening of the oxidation chamber has to be removed.

The isothermal pumping power for the idealized case is

$$P_{\text{pump,vacuum}} = \dot{n}_{\text{O}_2} \mathcal{R} T_{\text{pump}} \ln\left(\bar{p}_{\text{O}_2}{}^{-1}\right) \quad (18)$$

The molar flow rate of oxygen $\dot{n}_{\text{O}_2}$ is calculated from stoichiometry of the overall reaction as half of the flow rate of evolving carbon monoxide, the temperature T_{pump} of the vacuum pump is assumed to be the ambient temperature and $\bar{p}_{\text{O}_2}$ is the partial

pressure of oxygen in the reduction chamber. The realistic pumping work is calculated through fitting a function to actual vacuum pump power consumption data provided by a manufacturer (Personal communication with Pfeiffer Vacuum and J. Felinks, DLR), where the derivation is not shown here. Especially towards lower pressures, the required power for pressure reduction shows a strong deviation from the theoretical limit. Also for the CO/CO_2 separation a theoretical and a practically relevant description of the required power input is chosen. For the idealized case, the thermodynamic separation work is

$$P_{\mathrm{sep,CO/CO_2}} = \left(\dot{n}_{\mathrm{CO}} + \dot{n}_{\mathrm{CO_2}}\right)\mathcal{R}T_0\left(c_{\mathrm{CO}}\ln\frac{1}{c_{\mathrm{CO}}} + \left(1-\frac{1}{c_{\mathrm{CO}}}\right)\ln\frac{1}{(1-c_{\mathrm{CO}})}\right). \qquad (19)$$

The separation is assumed to be complete, *i.e.* pure streams of CO and CO_2 are produced. This level of purity may not be required for the syngas conversion but represents the ideal case of complete oxidant recycling and undisturbed FT reaction and is therefore assumed here. For the case of the practically relevant separation work, literature data for the capture of CO_2 from a flue gas stream from a fossil power plant have been chosen as a reference. 132 kJ of heat and 9 kJ of electricity are thus required for the capture of one mol of CO_2 (Zeman, 2007).

The efficiency of the reactor is defined as

$$\eta = \frac{\text{chemical energy stored in product}}{\text{solar power into reactor} + \text{ auxiliary power}} = \frac{\dot{n}_{\mathrm{CO}}\mathrm{HHV}_{\mathrm{CO}}}{\dot{Q}_{\mathrm{solar}} + P_{\mathrm{aux}}}. \qquad (20)$$

285 This definition assumes the energy input to the reactor to be accounted at the system
286 boundary of the reactor, *i.e.* the concentration efficiency and the primary energy
287 conversion efficiency for auxiliary power can be included depending on the chosen
288 technologies. Contrary to other publications this gives a wider definition of efficiency as
289 no additional constraint on the energy conversion process has to be made.
290
291 The temperature of the ceria pieces in the heat exchanger is calculated with an energy
292 balance of the single chambers (exemplary chamber shown in Fig. 2), where a transient
293 lumped parameter model with (*n*-2) control volumes, each subdivided into upper and
294 lower chamber halves, is used to calculate the steady state. Heat is transferred between
295 the upper and lower chamber half through radiation and heat is lost to the environment
296 through convection and radiation, where the outer wall temperature of the heat exchanger
297 is assumed to have a constant temperature of 373 K and the wall emissivity to be 0.5.
298 The energy balance of the element in one chamber half of the heat exchanger is

$$\frac{dE}{dt} = mc_{p,\mathrm{CeO_2}}\frac{dT}{dt} = \mp\dot{Q}_{\text{heat exchange}} - \dot{Q}_{\text{loss,rad}} - \dot{Q}_{\text{loss,conv}}, \quad (21)$$

299
300 where the negative sign in front of the net heat exchange rate is for the upper chamber
301 and the positive sign is for the lower chamber half.
302 The radiation heat transfer to the adjacent half of the chamber is modeled with
303

$$\dot{Q}_{\text{heat exchange}} = \frac{A_{\text{he,int}}\sigma\left(T_{k,\text{u}}^4 - T_{k,\text{l}}^4\right)}{\frac{1}{\varepsilon_\text{u}} + \frac{1}{\varepsilon_\text{l}} - 1}, \quad (22)$$

i.e. the formula for heat exchange between parallel flat plates with a view factor of 1 due to the close proximity (Diver et al., 2008; Howell et al., 2011). σ is the Stephan-Boltzmann constant, $T_{k,u}$ and $T_{k,l}$ are the temperatures of the upper and lower half of the *k*-th chamber, respectively. The emissivities ε_u and ε_l are both functions of temperature (Touloukian et al., 1971). The heat propagation into the material is assumed to proceed at a rate large compared to the rate of radiative heat exchange. This is approximately the case *e.g.* for materials with a high thermal conductivity, a low thermal mass, a favorable geometry or intra-chamber intermixing particles. In a concrete technical realization, the propagation of heat in the material depends on the geometry, the porosity and density of the material, besides others, and can, depending on its value, significantly influence the heat exchanger efficiency, as will be shown in an example below. Firstly, however, to gain fundamental insight into the upper bound of efficiency and in order not to limit the model to the analysis of specific system realizations, the assumptions above are chosen.

From basic geometry, the total length of the heat exchanger is $L_{\text{he,total}} = (n-2) \times L_{\text{chamber}}$, where $L_{\text{chamber}} = \sqrt{A}$ for the assumed cubic shape of a single chamber, the total internal area is $A_{\text{he,int,total}} = (n-2) \times A$, the total area facing the environment is

322 $A_{\mathrm{he,ext,total}} = 6 \times A_{\mathrm{he,int,total}}$. For a single chamber half, the external area $A_{\mathrm{he,ext}}$ is thus
323 three times the internal area $A_{\mathrm{he,int}} = A$.
324 Radiation heat transfer from the reactor wall to the environment is
325

$$\dot{Q}_{\mathrm{loss,rad}} = \varepsilon_{\mathrm{wall}} A_{\mathrm{he,ext}} \sigma (T_{\mathrm{wall}}^4 - T_0^4). \quad (23)$$

326
327 Heat loss to the environment by convection is
328

$$\dot{Q}_{\mathrm{loss,conv}} = \alpha A_{\mathrm{he,ext}} \Delta T = \alpha A_{\mathrm{he,ext}} (T_{\mathrm{wall}} - T_0), \quad (24)$$

329
330 where the convective heat transfer coefficient α is taken to be 15 W m^{-2} K^{-1} (Hischier et
331 al., 2009).
332 Starting from a first guess of the temperature distribution in the heat exchanger, the
333 parallel calculation of temperature evolution in all heat exchanger chambers is continued
334 until a steady state is reached, *i.e.* until the maximum change in temperature of the
335 control volumes after two consecutive time steps is smaller than 0.01 K.
336
337
338

3. MODEL VALIDATION

To give credibility to the proposed model, its results shall be compared with data from the recent literature. As comparable models have been introduced recently that describe reactor concepts using also a more generic approach, a validation by comparison with these data is sought. For this purpose, the presented model is adapted to describe the respective literature model to allow for a comparison of results. Two models are chosen for the comparison. The first literature model is the particle reactor concept by Ermanoski *et al.* (Ermanoski et al., 2013). The changes made to the generic model comprise an adjustment of chamber number and residence time to match the recuperation efficiency, the adaption of a similar formulation of efficiency, the assumption of complete reoxidation of the material at the prescribed oxidation temperature, and the choice of identical system parameters such as temperatures, pressures and component efficiencies, besides others. The mean absolute deviation between the calculated efficiency and the literature values is 1.5%.

The second literature model is a simpler model by Chueh and Haile (Chueh and Haile, 2010), where a batch reactor concept without heat recuperation is assumed. In the generic reactor model, the chamber number is set to two to exclude internal heat recuperation, gas heat recuperation is set to zero, thermodynamics of the oxidation reaction are taken into account, system parameters are set equally and an identical formulation of efficiency is chosen. The mean absolute deviation between the calculated efficiency and the literature values is 1.2%. The comparison with two literature models thus shows a very good

361 agreement, validates the chosen approach and demonstrates the wide range of
362 applicability of the model in the description of very diverse solar reactor concepts.
363
364

4. MODEL DEMONSTRATION

In the following, the applicability of the model shall be demonstrated with an example. The exemplary system has a ceria mass of 1 kg per piece with an area of 0.01 m² facing the other chamber half, a concentration ratio of 3000 suns, a vacuum pump to reduce the oxygen partial pressure to 10^{-3} atm, an oxidation pressure of 1 atm and a gas heat recovery efficiency of 95%. Preliminary calculations found that 80 chambers constitute a system close to the optimum which is why this number of chambers is chosen here. The total length of the heat exchanger is then $78 \times \sqrt{A} = 7.8$ m, its internal area is $78 \times A = 0.78\ \mathrm{m}^2$ and its external area is $6 \times 78 \times A = 4.7\ \mathrm{m}^2$. The other system parameters can be taken from Table 1. Mass loss of oxidant due to the opening of the oxidation chamber which is at a higher pressure than the other chambers is accounted for. A value of $f_{\mathrm{CO}_2} = 2$ has been chosen in order to increase efficiency (Chueh and Haile, 2010).

The temperature distribution in the chambers is as seen in Fig. 3, with the temperature in the upper chambers (going from the reduction chamber to the oxidation chamber) falling from $T_{\mathrm{H}} = 1800$ K to 1078 K and in the lower chambers (opposite direction) rising from $T_{\mathrm{L}} = 1000$ K to 1599 K. The efficiency η_{he} of the heat exchanger thus is 73.7%. In general, this efficiency is a function of number of chambers, residence time and the entry temperatures, besides others. Here, we assume one piece at a time in the reduction and one in the oxidation chamber only. However, the degrees of freedom of the model could be increased by allowing a larger number of pieces in the reaction chambers, decoupling

386 the residence time in the heat exchanger from the residence times in the reaction
387 chambers.
388
389 The energy balance normalized to the amount of carbon monoxide produced is shown in
390 Fig. 4. The largest part of the energy input is required to heat ceria in spite of a heat
391 recuperation efficiency of more than 70% in the heat exchanger. Effective heat
392 recuperation is especially important in nonstoichiometric cycles because, compared to
393 stoichiometric cycles, the mass of reactive material to be heated per mol of fuel produced
394 is large. The next largest items in the energy budget are the reduction enthalpy and
395 energy lost due to reradiation. Absolute reradiation losses strongly increase with
396 reduction temperature, however, the increased reduction temperature also leads to higher
397 amounts of CO produced, decreasing the normalized reradiation losses. Due to these two
398 adverse effects, the reradiation losses normalized to the amount of fuel produced are
399 stabilized with respect to increasing reduction temperatures.
400 For the vacuum pump and the gas separation, the black bars show the ideal
401 thermodynamic minimum and the grey bars show the realistic values as derived above.
402 The assumed thermodynamic work only contributes insignificantly to the overall energy
403 balance while the practically more relevant values increase the relative impact of vacuum
404 pumping and gas separation considerably. The common assumption in literature of the
405 thermodynamic minimum work is therefore likely to underestimate actual values and thus
406 their influence on the energy balance (see *e.g.* (Ermanoski et al., 2013)). Heating of the
407 oxidant carbon dioxide does not influence the energy balance significantly. Heat

recuperated from the gases leaving the reactor reduces the required concentrated solar radiation input as the energy can be used to preheat incoming gases. However, due to the relatively small oxygen nonstoichiometry and as the oxidant flow rate is chosen proportional to the evolving oxygen, energy stored in the sensible heat of the gases presents only a minor contribution, even though the recovery rate has been chosen high with 95% efficiency (as in (Bader et al., 2013; Ermanoski et al., 2013)).

When reduction is performed at higher temperatures, the oxidation temperature should be increased as well. The reason for this is that two adverse effects occur: when the temperature swing is increased, a higher energy penalty due to oxide heating follows. On the other hand, a lower oxidation temperature favors reoxidation of the material and thus enhances productivity of the cycle. For the given system, a raise in reduction temperature thus leads to a higher oxidation temperature to maximize overall efficiency.

In Fig. 5, efficiency is shown as a function of reduction temperature T_{H} for oxygen partial pressures between 10^{-5} atm and 1 atm during reduction, where the ideal case assuming minimum thermodynamic work for vacuum generation and gas separation is shown with the dashed lines and the case based on more realistic efficiencies is shown with the solid lines. The pressure in the oxidation chamber is 1 atm and the oxidation temperature has been optimized on basis of the ideal case, as discussed above. All other parameter values can be taken from Table 1. Depending on the pressure in the reduction chamber, deviations are visible between the ideal and the realistic efficiencies: with decreasing pressure the actually required pumping work differs to a large degree from the theoretical

value, becoming limiting for the lowest pressure shown. This is due to a rapid decline of the pump efficiency with decreasing pressure for the realistic case as opposed to the logarithmic progression of the thermodynamic minimum for the ideal case, resulting in large deviations in the reactor efficiency. In fact, the highest efficiency for the ideal case is reached for the lowest pressure as also shown in literature (Ermanoski et al., 2013), however, the realistic case reaches its highest efficiency at a pressure of about 1-10 mbar. Below this value the required energy input for the pressure reduction becomes excessive. Towards higher reduction temperatures, the deviation between the ideal and realistic cases increases due to the larger oxygen flow rate that has to be removed and the associated pumping work. This result shows clearly that much could be gained from the development of more efficient pumps. As vacuum pumping is a mature technology, it remains to be determined where the technical limit of efficiency is.

As expected, efficiency is enhanced with rising reduction temperatures. This is due to the exponential increase in oxygen nonstoichiometry with temperature at constant oxygen partial pressure, as can be seen in (Garnier et al., 1975), which outweighs growing losses with temperature, such as reradiation losses or heating of the oxide and gases.

The largest efficiencies for the ideal case are reached at the highest reduction temperature and the lowest oxygen partial pressure: at $T_{\mathrm{H}} = 2000\,K$ and $\bar{p}_{\mathrm{O}_2} = 10^{-5}$, $\eta = 0.39$, while the largest efficiency in the realistic case is $\eta = 0.24$ at $T_{\mathrm{H}} = 2000\,K$. From a practical point of view, however, such high temperatures may not be achievable due to maximum temperature constraints in reactor engineering and material use with respect to

mechanical stability of the porous structure and sublimation, for example (Furler et al., 2012a). The effective limit of efficiency is therefore lower than the mathematical limit.

For a given number of chambers and residence time and otherwise constant parameters, the reduction and oxidation temperatures define the heat exchanger efficiency. The reason for this is that heat exchange is achieved through radiation between the hot and cold ceria pieces which is a function of the delta of the fourth power of their temperatures. Also, the heat capacity of ceria is temperature dependent. In Fig. 6, the heat exchanger efficiency η_{he} as defined in Eq. 14 is shown as a function of reduction and oxidation temperatures. The other parameters may be taken from Table 1. In the analyzed temperature regime, higher oxidation temperatures increase heat exchanger efficiency. This is partly due to the temperature dependent emissivity of the material having higher values at elevated temperatures which enhances heat transfer (Felinks et al., 2014; Touloukian et al., 1971). Also with increasing reduction temperatures, the heat exchanger works more efficiently: at $T_{\mathrm{H}} = 2000\,K$, a value exceeding $\eta_{\mathrm{he}} = 0.80$ can be reached. This is due to the fact that at higher temperatures, the emitted radiative power from a ceria piece increases proportional to the fourth power of temperature, enhancing overall heat transfer. If the oxidation temperature is fixed, the heat exchanger efficiency can be increased simply by raising the reduction temperature. This is due to the bidirectional heat exchange between hot and cold pieces: there is no penalty in increasing the reduction temperature as the heat transfer from the hot to the cold piece will be enhanced due to increased radiative power from the former to the latter. High heat exchanger efficiencies

473 substantially reduce the required energy input from solar energy and thus increase overall
474 efficiency.
475 Thermodynamics of the fuel production cycle are critically dependent on the
476 temperatures and oxygen partial pressures prevalent during oxidation and reduction. In
477 order to increase the productivity of the cycle per unit mass of ceria, it may be required to
478 reduce the temperature below the optimal value of the heat exchange process. The
479 penalty that follows for the recuperation may be outweighed by the benefit of increased
480 fuel productivity. The optimization of cycle efficiency is thus a trade-off between
481 multiple mechanisms, which is also the reason why overall efficiency is maximized at
482 different oxidation and reduction temperatures than which were calculated for maximum
483 heat recuperation efficiency.
484 In Fig. 7, overall cycle efficiency is calculated as a function of T_{L} and T_{H} for both the
485 idealized and realistic assumptions for vacuum pump power and gas separation.
486 Obviously, a higher reduction temperature increases efficiency, where penalties from
487 increased energy requirements from the larger temperature swing and reradiation are
488 compensated by enhanced fuel productivity. The influence of the higher energy
489 requirements for gas separation and vacuum generation for the realistic case are clearly
490 visible: a higher reduction temperature of about 30 K is required to reach an efficiency of
491 10% while towards higher efficiencies, this required temperature increase over the ideal
492 case becomes larger. Within the analyzed temperature regime, efficiencies of 30% and
493 above can only be reached with the idealized assumptions.
494

In order to analyze the influence of heat transfer within the reacting medium in the heat exchanger and to give an example of the applicability of the generic model with respect to a practically relevant case, the model is modified in the following way. The reactive medium is assumed to have a thickness of 0.05 m at a porosity of 0.8, a mean pore diameter of 2.5×10^{-3} m (Furler et al., 2014; Suter et al., 2014), and a mass of 0.77 kg. Alumina insulation thickness is 0.05 m and the thickness of the reactor wall made from Inconel 600 is 3×10^{-3} m. In the porous ceria and alumina insulation, heat is transferred by radiation and conduction, where the former is modeled with the Rosseland Diffusion Approximation as for example in Mey et al., 2013; Petrov, 1997; Wang et al., 2013; Zhang et al., 2007 and the latter is modeled with a modified form of the three resistor model (Suter et al., 2014). Material properties are taken from (Riess et al., 1986; Special Metals, 2015; Touloukian et al., 1975, 1971; Zircar Zirconia, 2015). The finite difference method is used for the discretization of the porous domains of ceria and insulation which are subdivided into a number of layers with constant properties. Five layers both in the ceria and the insulation domain are chosen after a grid convergence study showed convergence of the results with increasing number of layers and the results deviate by less than 0.2% from the calculation with the four-fold number of layers at a ten times smaller time step. A one-dimensional transient heat transfer model is thus formulated that solves the system of coupled nonlinear equations with the explicit Euler method. A comparison of the generic model with the more complex model for a heat exchanger with 10 chambers, a residence time of 10 s per chamber, and a mass of 0.77 kg per ceria piece gives heat exchanger efficiencies of 0.422 and 0.295, respectively. This indicates that

heat propagation through the porous media may have a significant influence on overall heat transfer and hence heat exchanger efficiency and has to be evaluated in each specific reactor realization.

CONCLUSIONS

In the recent literature, analyses of the fundamental efficiency potential and of specific reactor designs for solar thermochemical syngas production have appeared. Information about the ultimate efficiency limit of all concepts and about the expected performance of detailed reactor designs can therefore be found. With the generic approach presented here, a new path is proposed to the discussion that analyzes the wide design space of solar reactors and that can give information about practically relevant concepts. The model is presented for two-step redox reactions of solid reactive elements moving in a counter-flow arrangement between reduction and oxidation chambers for the production of solar syngas. Through this arrangement, solid heat recuperation is implemented by radiation heat exchange between reduced and oxidized elements. The reduction and oxidation reactions are modeled under the assumption of thermodynamic equilibrium and species conservation to calculate the achieved nonstoichiometry and the amount of fuel produced. The internal solid heat exchange process is calculated with a lumped parameter model using energy conservation involving radiation heat exchange between reduced and oxidized elements and losses to the surroundings.

As a model demonstration, an exemplary system is analyzed with 80 chambers and a

539 residence time of 10 s at a reduction temperature of 1800 K and an oxidation temperature
540 of 1000 K, using a vacuum pump to decrease oxygen partial pressure. While an upper-
541 limit heat exchanger efficiency of about 80% is reached under the assumption of
542 idealized heat propagation inside of the material, the corresponding energy balance shows
543 the heat input for the temperature increase of the reactive material to be the largest item
544 nevertheless. For the vacuum pump and the gas separation, an idealized case with the
545 thermodynamic minimum of the energy requirements, and a practically relevant case with
546 efficiencies based on actual devices and literature data are used. Depending on the
547 oxygen partial pressure in the reduction chamber, the realistic assumptions can lead to a
548 considerably higher energy demand than in the idealized case. At the chosen conditions,
549 the efficiency of the exemplary system with an oxygen partial pressure of 10^{-3} atm is 22%
550 for the idealized case and 16% for the realistic case. In this formulation, the energy
551 conversion process to mechanical or electrical energy is not defined in order to give a
552 wider definition of efficiency. This should be taken into account when comparing the
553 results with other publications.
554 In order to analyze the influence of heat propagation in the porous reactive material and
555 insulation, radiation and conduction are modeled with the Rosseland diffusion
556 approximation and the three resistor model and heat exchanger efficiency is found to be
557 strongly dependent on internal heat transfer characteristics for the chosen physical
558 parameters, where the material was not yet optimized with respect to this effect.
559 In future work, the presented reactor model serves as a tool for both the identification of
560 promising efficiency potentials in the wide multi-dimensional design space of

561 thermochemical reactor concepts as well as for performance analyses of specific
562 realizations with the necessary adaptations to each concept.
563
564 **ACKNOWLEDGMENT**
565 The authors gratefully acknowledge the contribution of Valentin Batteiger and Arne
566 Roth. The research leading to these results has received funding from the European
567 Union Seventh Framework Program (FP7/2007-2013) under grant agreement no. 285098
568 − Project SOLAR-JET.
569
570
571
572

REFERENCES

Bader, R., Venstrom, L.J., Davidson, J.H., Lipiński, W., 2013. Thermodynamic analysis of isothermal redox cycling of ceria for solar fuel production. Energy and Fuels 27, 5533–5544. doi:10.1021/ef400132d

Chueh, W.C., Falter, C., Abbott, M., Scipio, D., Furler, P., Haile, S.M., Steinfeld, A., 2010. High-flux solar-driven thermochemical dissociation of CO2 and H2O using nonstoichiometric ceria. Science 330, 1797–1801. doi:10.1126/science.1197834

Chueh, W.C., Haile, S.M., 2010. A thermochemical study of ceria: exploiting an old material for new modes of energy conversion and CO2 mitigation. Philos. Trans. A. Math. Phys. Eng. Sci. 368, 3269–3294. doi:10.1098/rsta.2010.0114

Chueh, W.C., Haile, S.M., 2009. Ceria as a thermochemical reaction medium for selectively generating syngas or methane from H2O and CO2. ChemSusChem 2, 735–739. doi:10.1002/cssc.200900138

Diver, R.B., Miller, J.E., Allendorf, M.D., Siegel, N.P., Hogan, R.E., 2008. Solar Thermochemical Water-Splitting Ferrite-Cycle Heat Engines. J. Sol. Energy Eng. 130, 041001. doi:10.1115/1.2969781

Engineering Toolbox, 2014. Convective Heat Transfer [WWW Document]. URL www.engineeringtoolbox.com (accessed 2.1.14).

Ermanoski, I., Siegel, N.P., Stechel, E.B., 2013. A New Reactor Concept for Efficient Solar-Thermochemical Fuel Production. J. Sol. Energy Eng. 135, 031002. doi:10.1115/1.4023356

Felinks, J., Brendelberger, S., Roeb, M., Sattler, C., Pitz-paal, R., 2014. Heat recovery concept for thermochemical processes using a solid heat transfer medium. Appl. Therm. Eng. 73, 1004–1011. doi:10.1016/j.applthermaleng.2014.08.036

Furler, P., Scheffe, J., Gorbar, M., Moes, L., Vogt, U., Steinfeld, A., 2012a. Solar thermochemical CO2 splitting utilizing a reticulated porous ceria redox system. Energy and Fuels 26, 7051–7059. doi:10.1021/ef3013757

Furler, P., Scheffe, J., Marxer, D., Gorbar, M., Bonk, A., Vogt, U., Steinfeld, A., 2014. Thermochemical CO2 splitting via redox cycling of ceria reticulated foam structures with dual-scale porosities. Phys. Chem. Chem. Phys. 16, 10503–11. doi:10.1039/c4cp01172d

605 Furler, P., Scheffe, J.R., Steinfeld, A., 2012b. Syngas production by simultaneous
606 splitting of H2O and CO2via ceria redox reactions in a high-temperature solar
607 reactor. Energy Environ. Sci. 5, 6098. doi:10.1039/c1ee02620h

608 Garnier, J.E., Blumenthal, R.N., Panlener, R.J., Sharma, R.K., 1975. A thermodynamic
609 study on CaO- doped nonstoichiometric cerium dioxide. Solid State Commun.
610 doi:10.1016/0038-1098(75)90708-5

611 Hao, Y., Yang, C.-K., Haile, S.M., 2013. High-temperature isothermal chemical cycling
612 for solar-driven fuel production. Phys. Chem. Chem. Phys. 15, 17084–92.
613 doi:10.1039/c3cp53270d

614 Hischier, I., Hess, D., Lipiński, W., Modest, M., Steinfeld, a., 2009. Heat Transfer
615 Analysis of a Novel Pressurized Air Receiver for Concentrated Solar Power via
616 Combined Cycles. J. Therm. Sci. Eng. Appl. 1, 041002. doi:10.1115/1.4001259

617 Howell, J.R., Siegel, R., Mengüc, M., Pinar, R., 2011. Thermal Radiation Heat Transfer.
618 CRC Press, Boca Raton.

619 International Energy Agengy, 2014. 2014 Key World Energy STATISTICS.

620 Kim, J., Johnson, T. a., Miller, J.E., Stechel, E.B., Maravelias, C.T., 2012. Fuel
621 production from CO2 using solar-thermal energy: system level analysis. Energy
622 Environ. Sci. 5, 8417. doi:10.1039/c2ee21798h

623 Lapp, J., Davidson, J.H., Lipiński, W., 2013. Heat Transfer Analysis of a Solid-Solid
624 Heat Recuperation System for Solar-Driven Nonstoichiometric Cycles. J. Sol.
625 Energy Eng. 135, 031004. doi:10.1115/1.4023357

626 Lapp, J., Davidson, J.H., Lipiński, W., 2012. Efficiency of two-step solar thermochemical
627 non-stoichiometric redox cycles withheat recovery. Energy 37, 591–600.
628 doi:10.1016/j.energy.2011.10.045

629 Lapp, J., Lipinski, W., 2014. Transient Three-Dimensional Heat Transfer Model of a
630 Solar Thermochemical Reactor for H2O and CO2 Splitting Via Nonstoichiometric
631 Ceria Redox Cycling. J. Sol. Energy Eng. 136, 031006. doi:10.1115/1.4026465

632 Loutzenhiser, P.G., Meier, A., Steinfeld, A., 2010. Review of the Two-Step H2O/CO2-
633 Splitting Solar Thermochemical Cycle Based on Zn/ZnO Redox Reactions.
634 Materials (Basel). 4922–4938. doi:10.3390/ma3114922

635 Mey, S., Caliot, C., Flamant, G., Kribus, A., Gray, Y., 2013. Optimization of high
636 temperature SiC volumetric solar absorber. Energy Procedia 49, 478–487.
637 doi:10.1016/j.egypro.2014.03.051

638 Petrov, V. a., 1997. Combined radiation and conduction heat transfer in high temperature
639 fiber thermal insulation. Int. J. Heat Mass Transf. 40, 2241–2247.
640 doi:10.1016/S0017-9310(96)00242-6

641 Riess, I., Ricken, M., Noelting, J., 1986. Specific heat of non-stoichiometric ceria
642 (CeOy). Solid State Ionics 18-19, 725–726. doi:10.1016/0167-2738(86)90250-X

643 Roeb, M., Neises, M., Monnerie, N., Sattler, C., Pitz-Paal, R., 2011. Technologies and
644 trends in solar power and fuels. Energy Environ. Sci. doi:10.1039/c1ee01128f

645 Romero, M., Steinfeld, A., 2012. Concentrating solar thermal power and thermochemical
646 fuels. Energy Environ. Sci. 5, 9234. doi:10.1039/c2ee21275g

647 Special Metals, 2015. Inconel Alloy 600 [WWW Document]. URL
648 www.specialmetals.com/documents/Inconel alloy 600.pdf (accessed 6.1.15).

649 Stechel, E.B., Miller, J.E., 2013. Re-energizing CO2 to fuels with the sun: Issues of
650 efficiency, scale, and economics. J. CO2 Util. 1, 28–36.
651 doi:10.1016/j.jcou.2013.03.008

652 Steinfeld, A., Epstein, M., 2001. Light Years Ahead. Chem. Br. 37, 30–32.
653 doi:10.3929/ethz-a-004274060

654 Suter, S., Steinfeld, A., Haussener, S., 2014. Pore-level engineering of macroporous
655 media for increased performance of solar-driven thermochemical fuel processing.
656 Int. J. Heat Mass Transf. 78, 688–698. doi:10.1016/j.ijheatmasstransfer.2014.07.020

657 Touloukian, Y., Saxena, S., Hestermans, P., 1975. Thermophysical Properties of Matter-
658 the TPRC Data Series. Volume 11. Viscosity.

659 Touloukian, Y.S., Powell, R.W., Ho, C.Y., Klemens, P.G., 1971. Thermophysical
660 Properties of Matter - The TPRC Data Series--Vol.2. Thermal Conductivity -
661 Nonmetallic Solids. CINDAS/Purdue University.

662 U.S. Energy Information Administration, 2014. International Energy Outlook 2014.

663 Wang, F., Shuai, Y., Tan, H., Yu, C., 2013. Thermal performance analysis of porous
664 media receiver with concentrated solar irradiation. Int. J. Heat Mass Transf. 62,
665 247–254. doi:10.1016/j.ijheatmasstransfer.2013.03.003

666 Zeman, F., 2007. Energy and material balance of CO2 capture from ambient air. Environ.
667 Sci. Technol. 41, 7558–7563. doi:10.1021/es070874m

668 Zhang, B., Zhao, S., He, X., Du, S., 2007. High Temperature Thermal Physical Properties
669 of High-alumina Fibrous Insulation. J. Mater. Sci. Technol. 23, 860–864.

670 Zircar Zirconia, 2015. Fibrous Insulation - Type Buster M35 [WWW Document]. URL
671 http://www.zircarzirconia.com/product-literature/buster.php (accessed 1.1.15).

672

673

674

675

676 **Figure Captions List**

677

Fig. 1 Schematic of generic reactor model including *n* chambers, one each for reduction (*i*=1) and oxidation (*i*=*n*), and *n*-2 physical heat exchange chambers (*i*=2…*n*-1), each containing the mass *m* of reactive material.

Fig. 2 Schematic of upper and lower heat exchanger control volumes in the k-th chamber between two chamber openings, *i.e.* for $t\epsilon[\tau;\tau+\Delta t]$. Heat is transferred by radiation from the upper chamber at $T_{k,u}$ to the lower chamber at $T_{k,l}$ and energy is lost to the surroundings by radiation and convection.

Fig. 3 Temperature profile for generic reactor model with *n*=80 chambers and a residence time Δt of 10 s.

Fig. 4 Energy balance of generic vacuum reactor with n=80 chambers and a residence time Δt of 10 s. The two values shown for gas separation and pump power are based on the minimum thermodynamic work (black bars) and realistic efficiencies (grey bars). The oxidation temperature T_L is 1000 K and the reduction temperature T_H is 1800 K. Energy from gas heat recuperation is negative.

Fig. 5 Idealized (thermodynamic work for vacuum pump and gas separation assumed) and realistic (realistic efficiencies for vacuum pump and gas separation assumed) efficiency of generic vacuum reactor with *n*=80

chambers and a residence time Δt of 10 s as a function of reduction temperature T_H for different values of reduction oxygen partial pressure p_{O_2} (relative to standard state of 1 atm). The oxidation temperature is chosen such as to maximize efficiency.

Fig. 6 Contour plot of heat exchanger efficiency of generic vacuum reactor with n=80 chambers and a residence time Δt of 10 s as a function of oxidation temperature T_L and reduction temperature T_H.

Fig. 7 Contour plot of idealized (thermodynamic work for vacuum pump and gas separation assumed) and realistic (realistic efficiencies for vacuum pump and gas separation assumed) cycle efficiency of generic vacuum reactor with n=80 chambers and a residence time Δt of 10 s as a function of oxidation temperature T_L and reduction temperature T_H for a reduction oxygen partial pressure of 10^{-3}.

678

679

680 **Table Caption List**

681

Table 1 Parameter values for exemplary system

682

683

684

Fig. 1 Schematic of generic reactor model including *n* chambers, one each for reduction (*i*=1) and oxidation (*i*=*n*), and *n*-2 physical heat exchange chambers (*i*=2…*n*-1), each containing the mass *m* of reactive material.

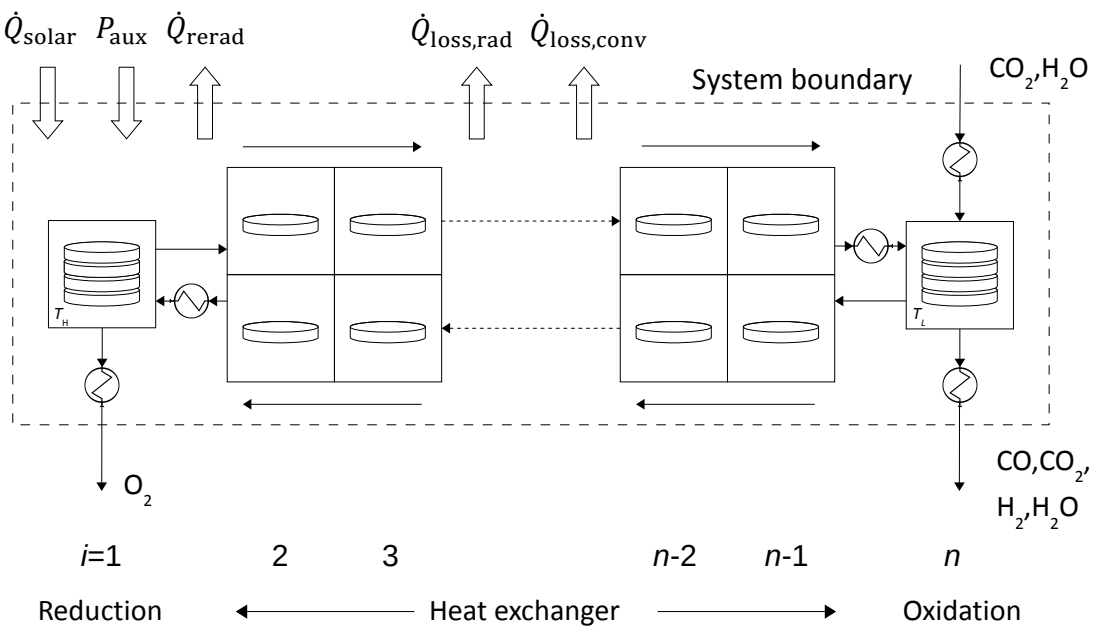

706 **Fig. 2** Schematic of upper and lower heat exchanger control volumes in the k-th chamber
707 between two chamber openings, *i.e.* for $t\epsilon[\beta\Delta t;(\beta+1)\Delta t]$. Heat is transferred by
708 radiation from the upper chamber at $T_{\mathrm{k,u}}$ to the lower chamber at $T_{\mathrm{k,l}}$ and energy is lost to
709 the surroundings by radiation and convection.

710

711

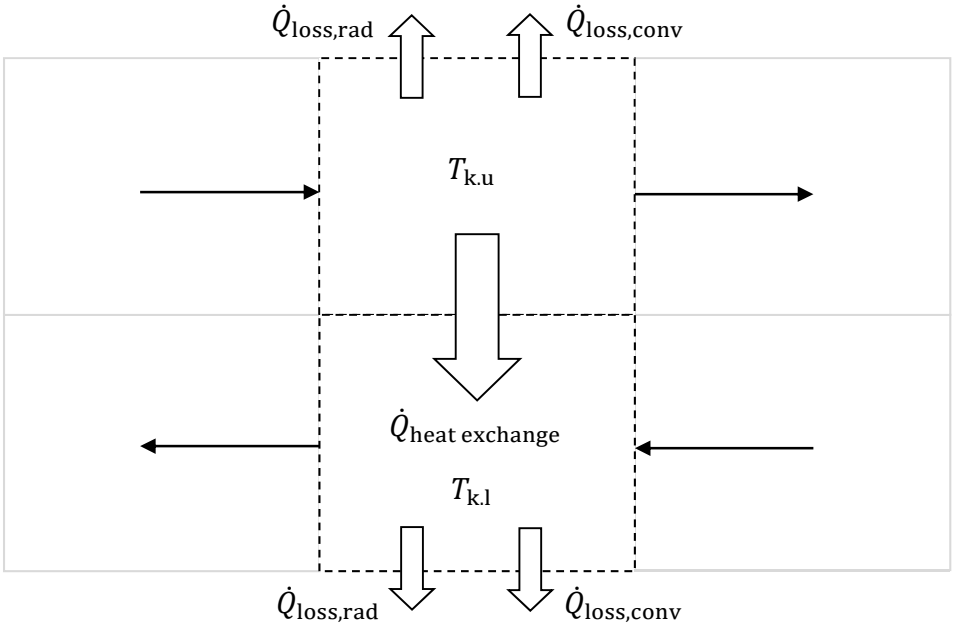

712 **Fig. 3** Temperature profile for generic reactor model with n=80 chambers and a residence
713 time Δt of 10 s and other parameters from Table 1.

714

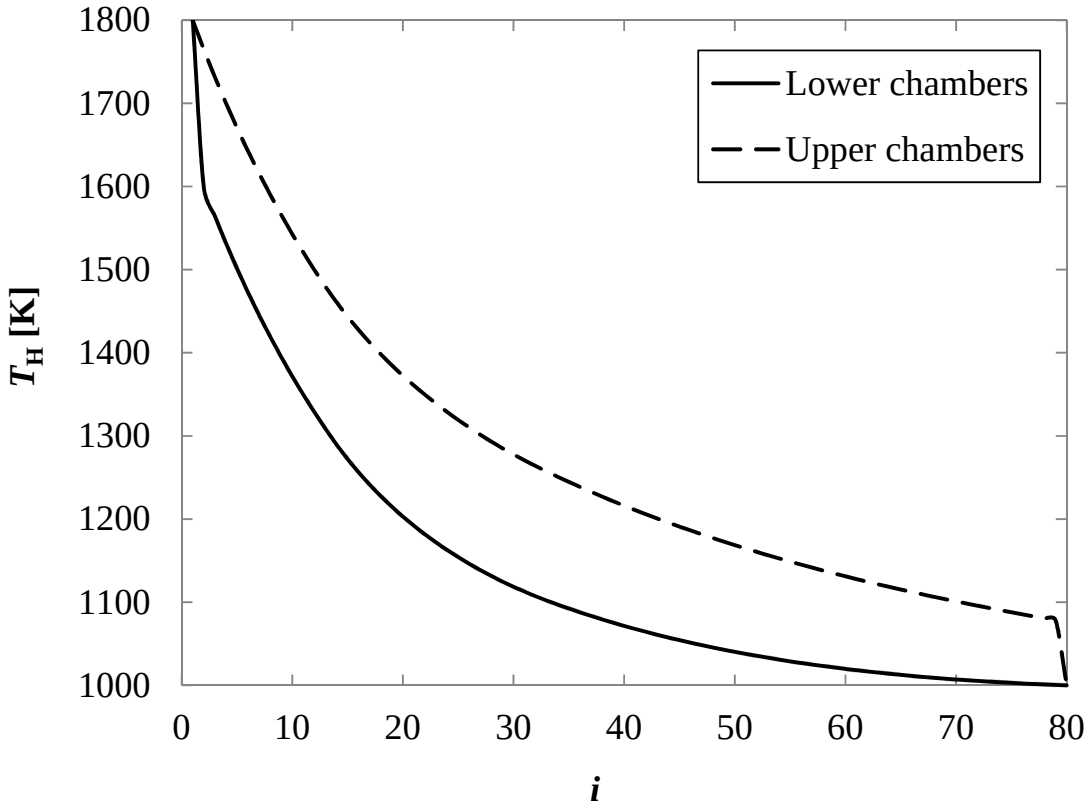

715

716

Fig. 4 Energy balance of generic vacuum reactor with n=80 chambers and a residence time Δt of 10 s. The two values shown for gas separation and pump power are based on the minimum thermodynamic work (black bars) and realistic efficiencies (grey bars). The oxidation temperature T_L is 1000 K and the reduction temperature T_H is 1800 K. Energy from gas heat recuperation is negative.

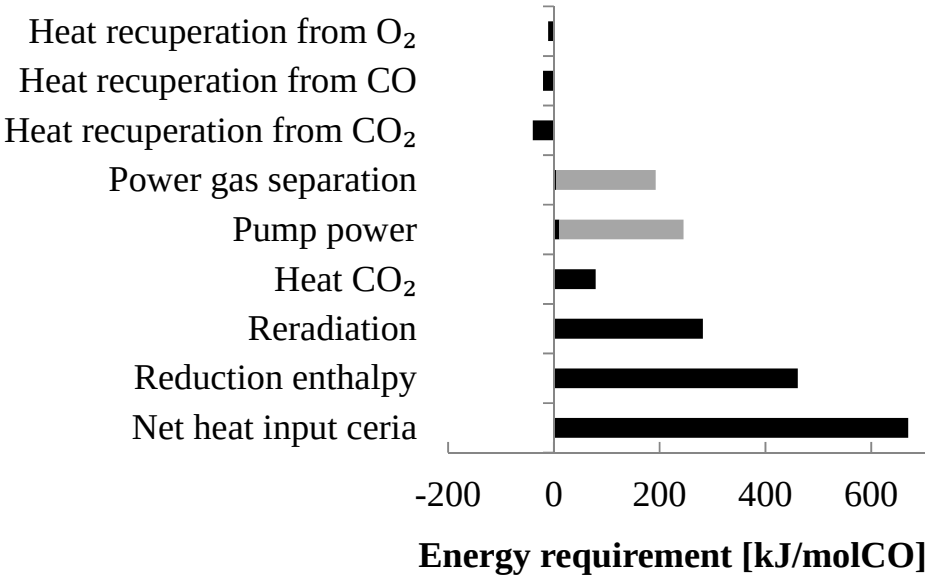

Fig. 5 Idealized (thermodynamic work for vacuum pump and gas separation assumed) and realistic (realistic efficiencies for vacuum pump and gas separation assumed) efficiency of generic vacuum reactor with n=80 chambers and a residence time Δt of 10 s as a function of reduction temperature T_{H} for different values of reduction oxygen partial pressure $\bar{p}_{O_2}$ (relative to standard state of 1 atm). The oxidation temperature is chosen such as to maximize efficiency.

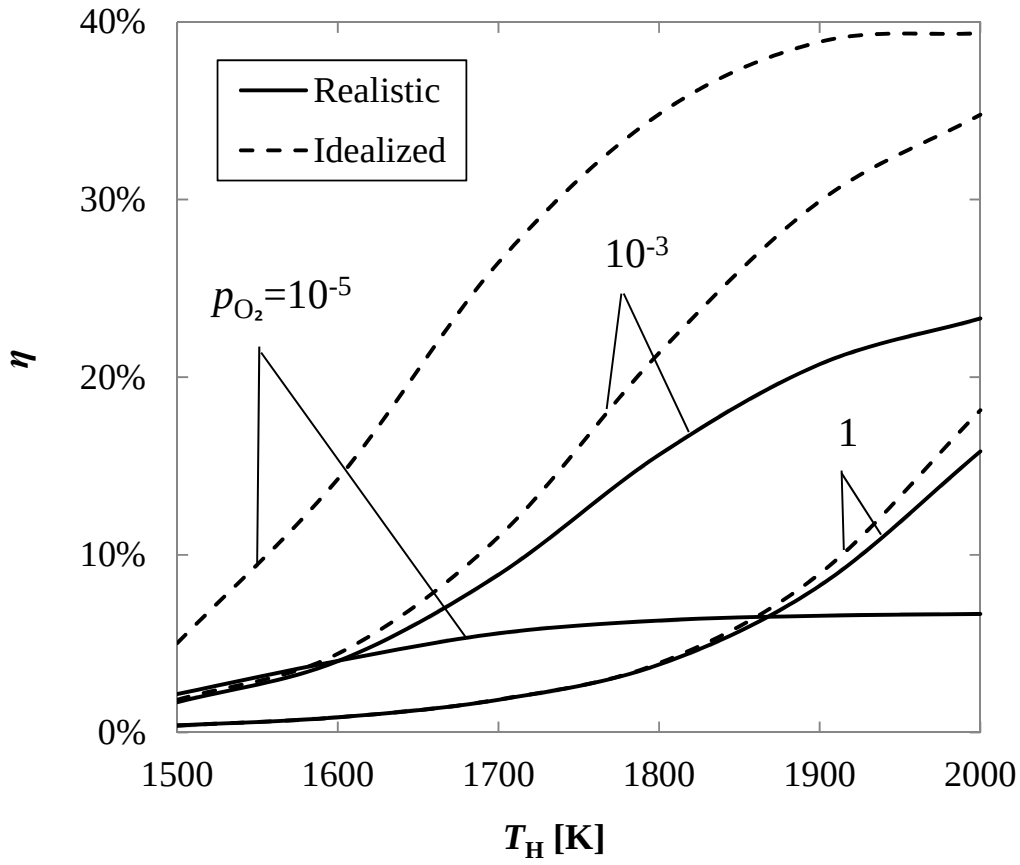

Fig. 6 Contour plot of heat exchanger efficiency of generic vacuum reactor with n=80 chambers and a residence time Δt of 10 s as a function of oxidation temperature T_L and reduction temperature T_H.

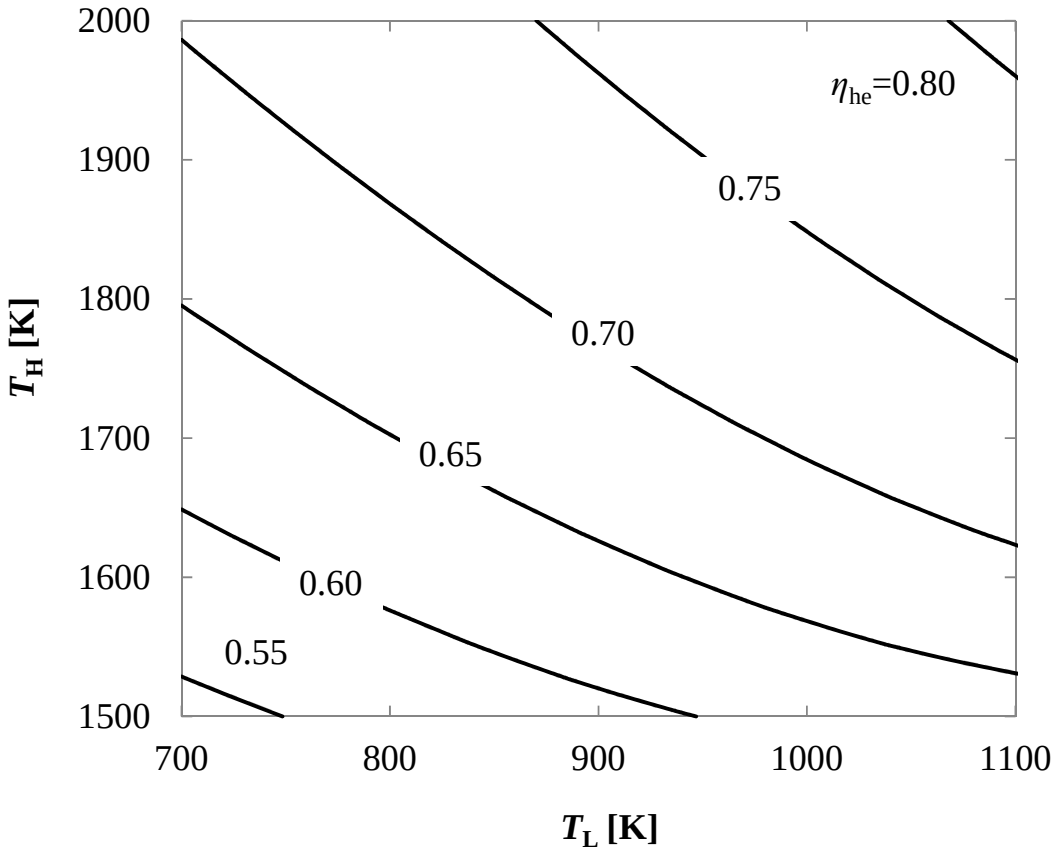

Fig. 7 Contour plot of idealized (thermodynamic work for vacuum pump and gas separation assumed) and realistic (realistic efficiencies for vacuum pump and gas separation assumed) cycle efficiency of generic vacuum reactor with n=80 chambers and a residence time Δt of 10 s as a function of oxidation temperature T_L and reduction temperature T_H for a reduction oxygen partial pressure of 10^{-3}.

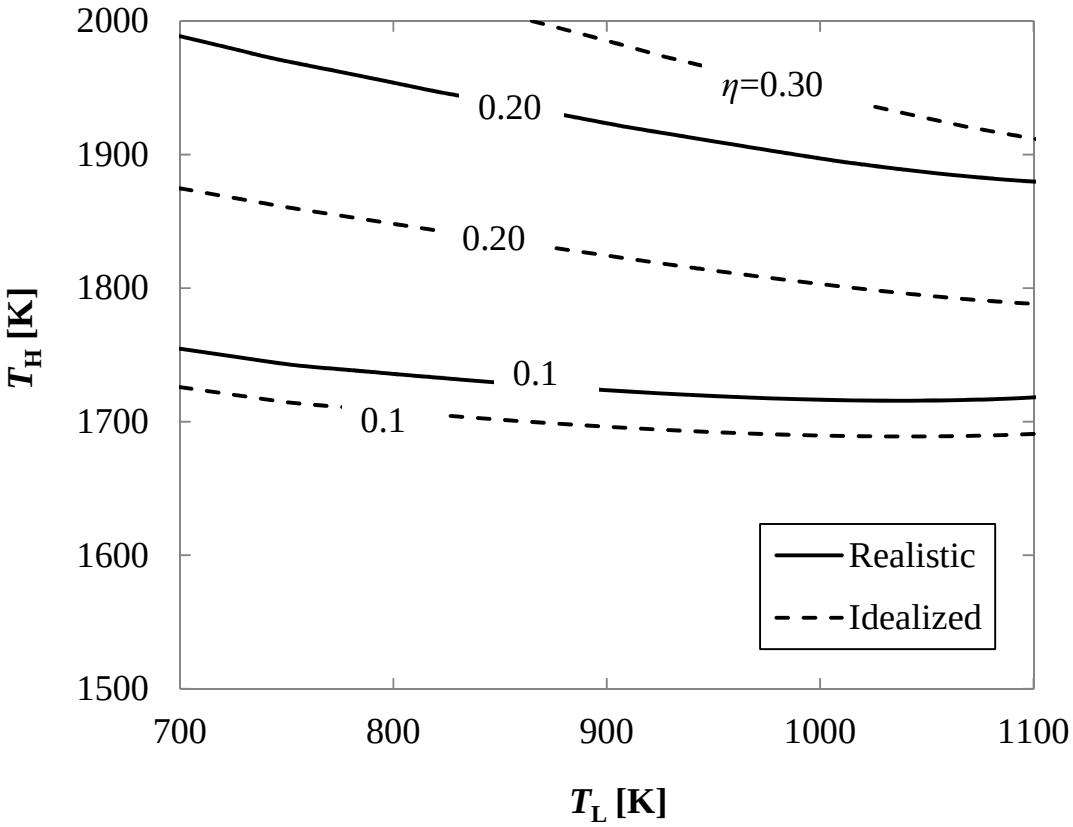

749 **Table 1** Parameter values for exemplary system
750

Parameter	Label	Value	Unit
Concentration ratio	C	3000	-
Oxidation temperature	T_L	1000	K
Reduction temperature	T_H	1800	K
Reduction pressure (relative to standard state of 1 atm)	$\bar{p}_{\mathrm{red}}$	10^{-3}	-
CO_2-flow (times min=δ_{red}) in oxidation chamber	$f_{\mathrm{CO_2}}$	2.0	-
Number of chambers	n	80	-
Residence time in heat exchanger	Δt	10	s
Mass of ceria piece	m	1.0	kg
Area of ceria piece facing other chamber	A	0.010	m^2
Efficiency of gas heat recovery	η_{gasrec}	0.95	-
Convective heat transfer coefficient	α	15	$W\ m^{-2}\ K^{-1}$

751

752